

See discussions, stats, and author profiles for this publication at: <https://www.researchgate.net/publication/270338893>

RAFT Dispersion Polymerization in Nonpolar Media: Polymerization of 3-Phenylpropyl Methacrylate in n -Tetradecane with Poly(stearyl methacrylate) Homopolymers as Macro Chain Transf...

ARTICLE *in* MACROMOLECULES · DECEMBER 2014

Impact Factor: 5.8 · DOI: 10.1021/ma502230h

CITATIONS

11

READS

38

4 AUTHORS, INCLUDING:



[Yiwen Pei](#)

Curtin University

19 PUBLICATIONS 152 CITATIONS

[SEE PROFILE](#)



[Andrew B. Lowe](#)

Curtin University

175 PUBLICATIONS 8,750 CITATIONS

[SEE PROFILE](#)

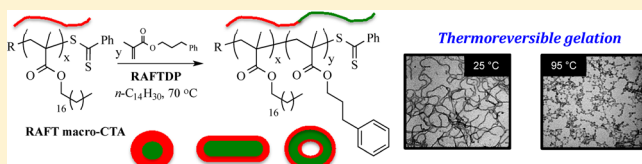
RAFT Dispersion Polymerization in Nonpolar Media: Polymerization of 3-Phenylpropyl Methacrylate in *n*-Tetradecane with Poly(stearyl methacrylate) Homopolymers as Macro Chain Transfer Agents

Yiwen Pei,* Luckshen Thurairajah, Odilia R. Sugita, and Andrew B. Lowe*

School of Chemical Engineering, UNSW Australia, Kensington, Sydney, NSW 2051, Australia

ABSTRACT: Poly(stearyl methacrylate) (PSMA) homopolymers, prepared by RAFT radical polymerization, have been employed in the RAFT dispersion polymerization (RAFTDP) of 3-phenylpropyl methacrylate (PPMA) in *n*-tetradecane. RAFTDPs yielded block copolymers with narrow molecular weight distributions and tunable compositions and allowed for ready access to different polymorphic nanoparticle phases.

Polymerization of PPMA at 20 wt %, for a fixed PSMA average degree of polymerization (\bar{X}_n) of 19, allowed for the *in situ* preparation of soft matter nano-objects with spherical, worm, and vesicular morphologies. For a fixed block copolymer composition increasing total solids (from 10 to 40 wt %) favored the formation of nanoparticles with higher ordered morphologies. For block copolymer samples that formed soft physical gels at ambient temperature, a macroscopic thermoreversible degelation–gelation phenomenon was observed. The fundamental reason for this was a worm-to-sphere morphology transition that was facilitated, in part, by the low glass transition temperature of the core-forming PPPMA block and an associated increase in the solvation of the core with increasing temperature. Finally, we note that degelation can also be effected by simple dilution with this macroscopic change now due to simple worm disentanglement and not a fundamental morphology transition.



INTRODUCTION

The ability of block copolymers to undergo self-directed assembly in a selective solvent is well documented.¹ Assembly occurs to give soft matter nanoparticles with, most commonly, a spherical morphology although higher ordered; more complex structures are also accessible.^{2–14} Traditionally, such self-assembled species are prepared by first synthesizing a well-defined block copolymer (most commonly, but not limited to, an AB diblock species) which, after characterization, is subjected to a processing step to give the nanoparticles. This may involve direct dissolution in a selective solvent or may require additional steps such as gradual stepwise dialysis against a selective solvent from a molecularly dissolved state. While these are well established and perfectly valid approaches to accessing polymeric nanoparticles, this is typically accomplished in dilute solution (≤ 1 wt % is common), and nano-objects other than spheres can be difficult to obtain.

Reversible addition–fragmentation chain transfer dispersion polymerization (RAFTDP)^{15–18} has recently been the topic of significant academic interest since it allows for the direct *in situ* preparation of self-assembled polymeric species of various morphologies (spheres, worms, and vesicles as the most common species) at high concentration (formulations at ≥ 50 wt % are readily achievable) in a one-pot process. The ease of execution and potential versatility of this technique have enabled the syntheses of a wide range of interesting nanoparticles in polar^{19–32} (typically aqueous or alcoholic solvents), nonpolar,^{33–36} and other, less common, media such as supercritical CO₂.^{37,38} Indeed, RAFTDP is now sufficiently

established that increasingly more complex formulations are beginning to be reported in the literature including the polymerization induced self-assembly of hybrid nanoparticles formed from two different macro-CTAs simultaneously,³² the synthesis of triblock-type species with a stimulus responsive block,³⁹ and recently an example of nanoparticles capable of undergoing a morphological transition as a function of pH.⁴⁰ However, there is still significant scope and opportunity for the evaluation of RAFTDP formulations employing previously unexamined conditions as well as new macro-CTA/comonomer pairings.

We have recently been interested in the ethanolic RAFTDP of various aryl methacrylates including 2-phenylethyl methacrylate,²⁹ certain aryloxy species,³¹ and 3-phenylpropyl methacrylate (PPMA).³⁰ PPMA is a particularly useful comonomer since, among other things, it possesses a subambient glass transition temperature (T_g), which can have a significant impact on the thermal responsive properties of nanoparticles with PPPMA in the core.

While polar-based RAFTDP formulations are now common, there are far fewer reports detailing RAFTDP in nonpolar media. Houillot and co-workers³³ reported the RAFTDP of methyl acrylate (MA) in isododecane utilizing a poly(2-ethylhexyl acrylate) (PEHA) macro-CTA (average degree of polymerization, $\bar{X}_n = 102$) at 20 wt % and 80 °C. While block

Received: November 2, 2014

Revised: December 3, 2014

Published: December 18, 2014



copolymer nanoparticles were obtained, all self-assembled species had a spherical morphology. This was likely a direct consequence of the large \bar{X}_n of the stabilizing PEHA macro-CTA. It has been observed by us, and others, that when the \bar{X}_n of the solvophilic block exceeds some critical value (this is highly system specific), the ability to access nanoparticle morphologies beyond spheres becomes extremely difficult even in block copolymers of extreme compositional asymmetry. Presumably, at some key \bar{X}_n steric stabilization becomes sufficient to preclude nanoparticle morphology transitions. However, what is clear is that this critical value is generally quite low ($\bar{X}_n < 30$ is common). However, full morphological transitions in nonpolar RAFTDP have been reported by Fielding et al. for block copolymers of poly(lauryl methacrylate) with poly(benzyl methacrylate) prepared in *n*-heptane at 90 °C.³⁴ With a poly(lauryl methacrylate) homopolymer with a relatively low \bar{X}_n of 17, the full common range of nanoparticles (spheres, worms, and vesicles) were readily obtained. In contrast, and consistent with the work by Houillot et al. noted above, for poly(lauryl methacrylate) macro-CTAs of higher \bar{X}_n (37 or above) only spherical species were observed with measured diameters ranging from 41 to 139 nm. Related to the work reported herein, Fielding and co-workers³⁶ detailed the RAFTDP synthesis of nanoparticles composed of poly(lauryl methacrylate-*b*-benzyl methacrylate) copolymer chains in *n*-dodecane at 70 °C. While the full common morphological range of nanoparticles were accessible in this formulation, the authors focused on the properties associated specifically with the worm nanoparticles and with an emphasis on their thermoresponsive properties.

Given our interest in PPMA as a comonomer in RAFTDP formulations, we have initiated studies evaluating its behavior in nonpolar RAFTDP systems. Herein we report our results regarding the RAFTDP of PPMA, with poly(stearly methacrylate) (PSMA) macro-CTAs in *n*-tetradecane. This is the first time PPMA has been employed as a comonomer in a nonpolar RAFTDP formulation and the first examples of such polymerizations conducted in this particular *n*-alkane.

EXPERIMENTAL SECTION

All reagents were purchased from the Aldrich Chemical Co. at the highest available purity and used as received unless noted otherwise. 2,2'-Azobis(isobutyronitrile) (AIBN) was purified by recrystallization twice from methanol and then stored in a freezer until needed. Stearyl methacrylate (SMA) and 3-phenylpropyl methacrylate (PPMA) were purified by passage through a column of basic alumina (3 times) and then stored in the freezer prior to use. 2-Cyanopropan-2-yl benzodithioate (CPDB) was stored in a freezer until needed.

RAFT Homopolymerization of Stearyl Methacrylate. Below is a typical procedure for the RAFT homopolymerization of stearyl methacrylate (SMA).

To a reaction vial equipped with a magnetic stir bar was added AIBN (3.87×10^{-2} g, 2.36×10^{-4} mol) and SMA (9.2 mL, 2.36×10^{-2} mol). In a separate vessel, CPDB (2.61×10^{-1} g, 1.18×10^{-3} mol) was dissolved in 7.6 mL of toluene. This solution was added to the AIBN, and then the vial was placed in a sonicator for ca. 30 min to ensure complete dissolution of the AIBN. The vial was then sealed with a rubber septum, and the solution purged with nitrogen gas while immersed in an ice bath. The vial was then placed in an oil bath preheated to 70 °C. Polymerization was allowed to proceed for 16 h after which it was halted by exposure to air while cooling in an ice water bath. The polySMA (PSMA) homopolymer was isolated by precipitation in an excess of MeOH. After filtration the homopolymer was redissolved in CHCl₃ and reprecipitated in MeOH distributed in four centrifuge tubes. After removal of the supernatant, the samples

were dried *in vacuo* overnight prior to NMR spectroscopic and SEC analyses.

RAFT Dispersion Polymerization of PPMA with PSMA_x in *n*-Tetradecane. Below is a typical procedure for the RAFTDP of PPMA with a PSMA₁₉ macro-CTA in *n*-tetradecane. All RAFTDPs were performed following this general procedure.

To a vial equipped with a magnetic stir bar were added AIBN (1.97 mg, 1.2×10^{-5} mol) and PPMA (0.404 g, 2.0×10^{-3} mol). The solution was then stirred allowing dissolution of the initiator in the monomer. To a second vial equipped with a stir bar was added PSMA₁₉ (0.4 g, 1.14×10^{-3} mol of SMA) and 4.22 mL of *n*-tetradecane. After complete dissolution of the PSMA₁₉ the solution was combined with the AIBN/PPMA solution. The vial was sealed with a rubber septum, and the solution purged with nitrogen. The vial was then placed in a preheated oil bath set to 70 °C for 24 h. Block copolymer was isolated by precipitation into a large excess of MeOH followed by filtration and drying overnight *in vacuo* at 40 °C prior to NMR spectroscopic and SEC analyses.

Nuclear Magnetic Resonance (NMR) Spectroscopy. NMR spectra were recorded on a Bruker 300 MHz spectrometer. ¹H NMR spectra were recorded in deuterated chloroform (CDCl₃), and sixty-four scans were averaged per spectrum. Residual CHCl₃ ($\delta = 7.26$ ppm) was used as the internal reference signal. Temperature-dependent NMR characterization analyses were performed using a Bruker Avance III 500 spectrometer (¹H, 500.13 MHz) equipped with a 31P-TBI probe utilizing 7500 Hz sweep width, 3.2 s acquisition time, and 2 s recycle delay. The pulse program employing solvent suppression at a ¹H chemical shift was used to eliminate the solvent peak. Samples were heated up from 25 to 105 °C and allowed to equilibrate at each temperature for at least 10 min prior to measurements. Variable temperature NMR studies were performed in fully deuterated *n*-tetradecane (d_{30} -*n*-tetradecane).

Size Exclusion Chromatography (SEC). SEC analysis was conducted on a Shimadzu modular system consisting of an autoinjector, a Polymer Labs 5.0 μm bead-size guard column (50 × 7.5 mm), three linear Polymer Labs columns (10^5 , 10^4 , and 10^3 Å), and a differential refractive index detector. THF was used as the mobile phase at a temperature of 40 °C and a flow rate of 1.0 mL min⁻¹. The system was calibrated with a series of narrow molecular weight distribution polystyrene standards with molecular weights ranging from 0.58 to 1820 kg mol⁻¹. The chromatograms were analyzed with Cirrus SEC software version 3.0. (Co)Polymer samples were prepared at a concentration of 3–5 mg mL⁻¹ and filtered through a 0.45 μm nylon filter prior to analysis.

Dynamic Light Scattering (DLS). Nanoparticle size distributions were determined on a Malvern Zetasizer Nano Series instrument (laser power = 4 mW, wavelength = 633 nm, detection angle = 173°). Samples for analysis were prepared by taking 50 μL of the block copolymer dispersion solution, diluted with 1.45 mL of *n*-tetradecane and filtered twice through 0.45 μm nylon filters. For temperature-dependent DLS analysis, samples were heated up and allowed to equilibrate at each temperature for at least 10 min prior to measurements.

Transmission Electron Microscopy (TEM). TEM analyses were conducted on a JEOL 1400 transmission electron microscope operating at 100 kV. 10 μL of block copolymer solution was added slowly to 1.49 mL of *n*-tetradecane under stirring. The copolymer solution (0.13% w/w) was dropped onto the top of a carbon-coated copper grid (ProSciTech) and allowed to dry for 1 min. Excess solution was wicked off using filter paper. Samples were then stained by exposure to RuO₄ vapor for 15 min at room temperature prior to analysis. As a heavy metal compound, ruthenium tetroxide (RuO₄) can interact with the core-forming PPPMA block to improve contrast. The ruthenium tetroxide was prepared as follows: ruthenium (IV) oxide hydrate (0.06 g) was added into a solution of sodium periodate (0.4 g) in water (10 mL) with stirring at 0 °C for 4 h. A yellow solution of ruthenium tetroxide was obtained at the end of reaction and was stored in the freezer prior to use. For TEM grid preparation at high temperature, all materials and equipment were placed in a hot oven at 95 °C for 10 min. The 20 wt % PSMA-*b*-PPPMA copolymer sample

Scheme 1. General Outline for the Synthesis of $\text{PSMA}_x-b\text{-PPPMA}_y$ Copolymer Nanoparticles via RAFTDP in *n*-Tetradecane at 70 °C

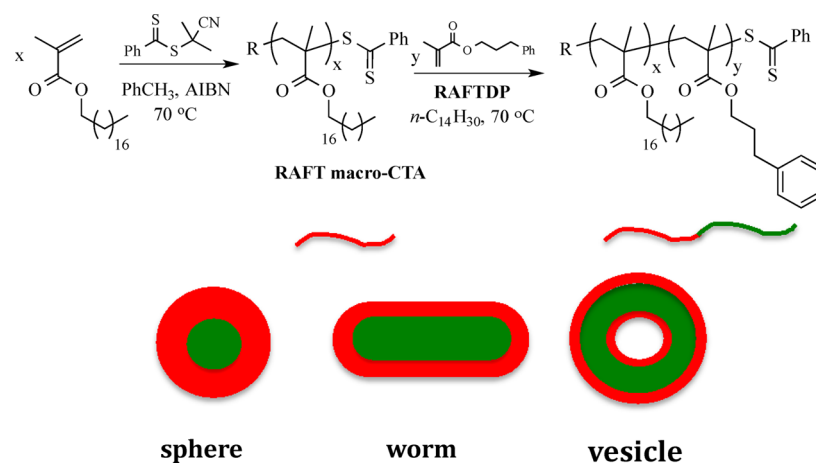


Table 1. Summary of PSMA–PPPMA Block Copolymer Compositions, PPMA Conversion, Molecular Weights Measured by ^1H NMR spectroscopy and Size Exclusion Chromatography, SEC-Determined Dispersities (D_M), Dynamic Light Scattering Measured Hydrodynamic Diameters (D_h) of Nanoparticles and Their Associated Polydispersities ($\text{PDI} = \mu_2/I^2$), and the TEM-Observed Nanoparticle Morphology. All Samples were prepared in *n*-Tetradecane at 20 wt % Solids and 70 °C for 24 h

composition ^a	PPMA/CTA/AIBN	PPMA conv ^a (%)	NMR MW ^b	SEC \bar{M}_n ^c	D_M ^c	DLS D_h ^d (nm)	DLS PDI	TEM morph ^e
PSMA ₁₉ - <i>b</i> -PPPMA ₃₃	35/1/0.2	98	13 400	9 500	1.15	17.8	0.004	S
PSMA ₁₉ - <i>b</i> -PPPMA ₄₇	50/1/0.2	98	16 250	10 900	1.17	21.7	0.003	S
PSMA ₁₉ - <i>b</i> -PPPMA ₆₈	72/1/0.2	96	20 500	16 000	1.16	243	0.26	S + W
PSMA ₁₉ - <i>b</i> -PPPMA ₈₅	90/1/0.2	96	24 000	16 800	1.17	217	0.31	W
PSMA ₁₉ - <i>b</i> -PPPMA ₈₇	95/1/0.2	94	24 400	17 000	1.16	345	0.24	W + V
PSMA ₁₉ - <i>b</i> -PPPMA ₉₈	105/1/0.2	96	26 700	20 400	1.16	498	0.27	V
PSMA ₁₉ - <i>b</i> -PPPMA ₁₆₅	180/1/0.2	92	40 400	28 500	1.17	1121	0.11	V

^aDetermined by ^1H NMR spectroscopy. ^bDetermined by ^1H NMR spectroscopy and end-group analysis. ^cMeasured in THF on a system calibrated with a series of narrow molecular weight distribution polystyrene standards. ^dMeasurements were made after appropriate dilution of the parent samples; see Experimental Section. ^eS = spheres, W = worms, V = vesicles. Morphology was determined after appropriate dilution of the parent sample to facilitate imaging.

was kept under continuous stirring at 95 °C for 10 min and then diluted to 0.13 wt % with warm *n*-tetradecane (at same temperature of copolymer sample) prior to TEM sample preparation. The TEM grids were then stained as described above.

RESULTS AND DISCUSSION

The overall approach to the target block copolymer nanoparticles is shown in Scheme 1. Stearyl methacrylate (SMA) was first homopolymerized in toluene under typical homogeneous RAFT conditions utilizing 2-cyanopropan-2-yl benzodithioate as the mediating agent to give two homopolymers with low, but comparable, average degrees of polymerization (\bar{X}_n) (PSMA₁₇ and PSMA₁₉ where 17 and 19 represent the \bar{X}_n 's). Both PSMA homopolymers had narrow molecular weight distributions with SEC-measured dispersities ($D_M = \bar{M}_w/\bar{M}_n$) of 1.15.

With the PSMA macro-CTAs available we proceeded to evaluate the RAFTDP of PPMA at a fixed total solids concentration of 20 wt %.

RAFTDP of PPMA with PSMA₁₉ for Variable \bar{X}_n of the PPPMA Block at 20 wt % Solids in *n*-Tetradecane. Table 1 gives a summary of the PSMA₁₉-PPPMA_y AB diblock copolymers prepared via RAFTDP in *n*-tetradecane, their compositions, experimentally determined molecular weights, dispersities, hydrodynamic diameters of the formed nano-objects, and observed nanoparticle morphology.

All RAFTDP block copolymer syntheses proceeded smoothly and yielded well-defined copolymers with increasing lengths of the PPPMA block. The polymerizations were generally more rapid in *n*-tetradecane than for those performed in a comparative study in *n*-octane.³⁵ This is consistent with a further observation regarding a lowering of the observed \bar{X}_n 's for the solvophobic block for a particular morphological transition (vide infra). The critical PPPMA chain length dictating the onset of self-assembly appears to be lower in *n*-tetradecane compared to *n*-octane. Since the onset of self-assembly is typically accompanied by an increase in the polymerization rate, it is this feature that is likely the cause for the observed faster polymerizations in *n*-tetradecane vs the lower *n*-alkane. In most instances, near-quantitative conversions of PPMA were attained after the 24 h polymerization period. The controlled nature of the block copolymerizations was evident from the measured SEC traces (Figure 1). The chromatograms are unimodal and symmetric with little-to-no evidence of high (dead polymeric species formed by macromolecular radical coupling side reactions) or low (macro-CTA) molecular weight impurities even in the most asymmetric species PSMA₁₉-*b*-PPPMA₁₆₅ (note: all SEC measurements were made after purification of the parent block copolymers by precipitation in MeOH to remove any residual PPMA monomer). Given the high conversions of PPMA, this is a gratifying result and is in contrast to some all-methacrylic

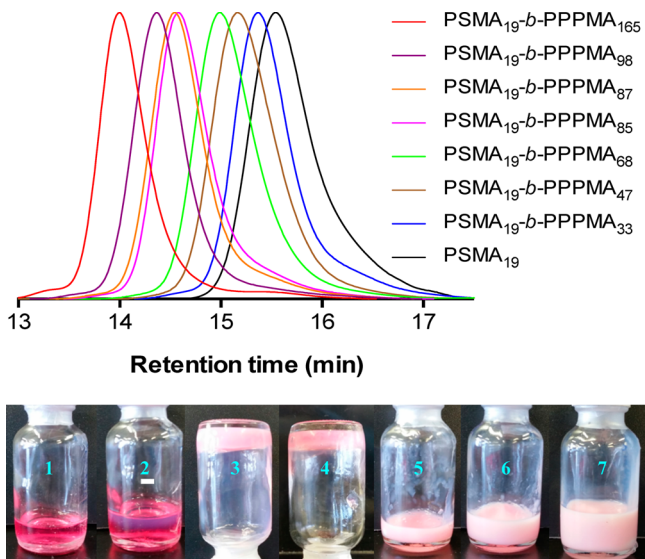


Figure 1. Experimentally measured size exclusion chromatograms for the series of PSMA₁₉-*b*-PPPMA_y block copolymers and the PSMA₁₉ macro-CTA demonstrating high blocking efficiency and the preparation of well-defined AB diblock copolymer solutions highlighting the change in the appearance of the solutions for the block copolymers listed with increasing PPPMA block length y (left to right, 33 to 165).

systems conducted in polar media where significant amounts of impurities have been reported to be present.^{31,41,42} The change in physical appearance of the solutions (see digital images Figure 1) with increasing length of the PPPMA block is typical for the formation of increasingly more complex self-assembled species (spheres then worms then vesicles). To evaluate this presumed evolution of nanoparticle morphology, small aliquots were extracted from the vials, diluted with *n*-tetradecane, deposited on a copper TEM grid, exposed to RuO₄ vapor, and

then imaged. Representative TEM images of the nanoparticles are shown in Figure 2.

For the PSMA₁₉-*b*-PPPMA₃₃ and PSMA₁₉-*b*-PPPMA₄₇ copolymers (Figure 2A shows an image of the latter) *in situ* self-assembly resulted in the formation of nanoparticles with a predominant spherical morphology although the latter block copolymer composition is clearly at the sphere–worm phase boundary. The DLS measured hydrodynamic diameters (D_h) of these two samples were 17.8 and 21.7 nm with very low associated DLS polydispersities of 0.004 and 0.003, respectively. An increase of the \bar{X}_n of the PPPMA block to 68 resulted in a mixed phase consisting of almost exclusively worm nanoparticles with contour lengths of ca. 100–200 nm and some spherical species (Figure 2B). We note that this sample also resulted in the formation of a solid, gelled material at room temperature (Figure 1, vial 3), a feature that will be discussed in more detail below. In the case of the PSMA₁₉-*b*-PPPMA₈₅ copolymer a pure worm phase was observed (Figure 1C), with the average contour length of the worm nanoparticles now being several hundreds of nanometers. This sample also existed as a physical gel at ambient temperature. While DLS data are given for these worm nano-objects, they should be treated as “sphere-equivalent” sizes given the assumptions associated with the Stokes–Einstein equation in DLS data analysis. Interestingly, increasing the \bar{X}_n of the PPPMA block by just 2 units to 87 results in the formation of another mixed phase that now consists of worms and vesicles (Figure 2D), while for all samples prepared with \bar{X}_n 's of the PPPMA block greater than this value resulted in the formation of essentially pure vesicular nanoparticles (Figures 2E and 2F), with sizes increasing for longer PPPMA block lengths. This was particularly true in the case of the PSMA₁₉-*b*-PPPMA₁₆₅ sample. The observed transitions from spheres to worms to vesicles (S–W–V) are consistent with the effect of increasing the solvophobic block length for a fixed \bar{X}_n of solvophilic stabilizing species of appropriate length. The morphology formed is, primarily,

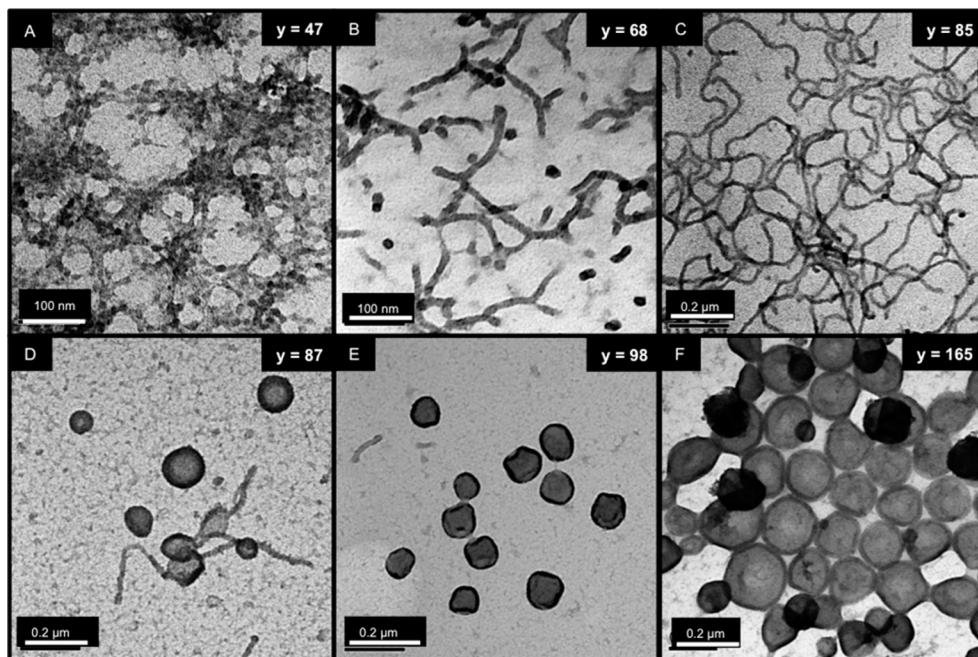


Figure 2. Representative TEM images of nanoparticles formed by PSMA₁₉-*b*-PPPMA_y block copolymers prepared in *n*-tetradecane at 20 wt % and 70 °C for (A) $y = 47$, (B) $y = 68$, (C) $y = 85$, (D) $y = 87$, (E) $y = 98$, and (F) $y = 165$.

Table 2. Summary of PSMA–PPPMA AB Diblock Copolymers, with the Same Targeted Composition, Prepared as a Function of Total Solids Concentration in *n*-Tetradecane at 70 °C, Comonomer Conversions, Molecular Weights As Determined by NMR Spectroscopy and SEC, Block Copolymer Dispersities, DLS Measured Hydrodynamic Diameters, and Polydispersities and the TEM Observed Nanoparticle Morphology

composition ^a	PPMA/CTA/AIBN	conc (wt %)	PPMA conv ^a (%)	NMR MW ^b	SEC \bar{M}_n ^c	D_M ^c	DLS D_h ^d (nm)	DLS PDI	TEM morph ^e
PSMA ₁₇ - <i>b</i> -PPPMA ₄₉	57/1/0.2	10	93	15 900	12 100	1.15	22.8	0.029	S
PSMA ₁₇ - <i>b</i> -PPPMA ₅₀	57/1/0.2	20	96	16 200	13 200	1.15	59.4	0.162	S + W
PSMA ₁₇ - <i>b</i> -PPPMA ₅₄	57/1/0.2	30	98	17 000	13 400	1.16	71.0	0.143	S + W
PSMA ₁₇ - <i>b</i> -PPPMA ₅₇	57/1/0.2	40	99	17 600	14 300	1.15	120	0.161	W

^aDetermined by ¹H NMR spectroscopy. ^bDetermined by ¹H NMR spectroscopy via end-group analysis. ^cMeasured on a system calibrated with a series of narrow molecular weight distribution polystyrene standards. ^dMeasurements were made after appropriate dilution of the parent samples; see Experimental Section. ^eS = spheres, W = worms. Morphology was determined after appropriate dilution of the parent sample to facilitate imaging.

dictated by the \bar{X}_n of the solvophobic block and is often rationalized in purely geometric terms (relative volume fractions of the individual blocks) employing the concept of the packing parameter, p , first developed by Israelachvili, Mitchell, and Ninham.⁴³ However, while qualitatively informative for polymeric soft matter nanoparticles, this should be treated with some caution since it was originally developed for the prediction of morphology in perfectly “monodisperse” low molecular weight surfactant systems. Additionally, geometric factors are not the only features that influence morphology, and it is important to consider other possible contributing factors such as the interfacial surface tension, the amorphous/crystalline/glassy nature of the core-forming block, i.e., its glass transition temperature (T_g), relative degrees of solvation of the core and coronal blocks, and the presence of ions/solution pH in the case of nanoparticles containing ionic functionalities.^{2,7,11,13,40,44}

The sequential transition through these different nanoparticle morphologies requires effective block copolymer chain mobility on a kinetically measurable time scale. Regardless of the transition, the block copolymer chains, and specifically those of the core-forming block, must be able to extricate themselves from a solvophobic environment, i.e., a spherical nanoparticle core, to facilitate rearrangement to higher ordered structures. While the formation of worm aggregates from spheres is assumed to occur via the 1D coalescence of spherical nanoparticles, the transition from worms to vesicles is more complicated and has been observed to proceed via numerous intermediate, transient structures. For example, various intermediate species have been described in an aqueous RAFTDP formulation of poly(glycerol monomethacrylate-*b*-2-hydroxypropyl methacrylate) copolymers.⁴⁵ However, regardless of the transitional mechanism(s) between different nanoparticle morphologies, this particular formulation is clearly an effective approach for the synthesis of new and interesting self-assembled species in nonpolar media.

Finally, we note that compared to our complementary studies detailing the preparation of similar AB diblock copolymers in *n*-octane under otherwise identical conditions, the morphological transitions appear to occur at lower \bar{X}_n 's of the PPPMA block when prepared in *n*-tetradecane vs *n*-octane although the differences are not large.³⁵ Similar behavior has also been noted by Armes et al., who prepared poly(lauryl methacrylate-*b*-benzyl methacrylate) copolymer nanoparticles via RAFTDP in *n*-heptane and *n*-dodecane.^{34,36}

Effect of Total Solids Concentration for a Fixed PSMA_x-*b*-PPPMA_y Composition. While varying the \bar{X}_n of the solvophobic PPPMA block for a fixed \bar{X}_n of the solvophilic PSMA block is a convenient approach for accessing soft matter

nanoparticles of differing morphology, the same progression through different self-assembled states can also be accomplished by varying the total solids content of the formulation for a fixed block copolymer composition. This approach is, however, slightly more synthetically challenging since it requires the preparation of (near) identical block copolymers under different experimental conditions. To examine the effect of total solids on the observed nanoparticle morphology, we employed the PSMA₁₇ macro-CTA and targeted an \bar{X}_n of the PPPMA block of 57 in 10, 20, 30, and 40 wt % formulations in *n*-tetradecane at 70 °C (Table 2). Conversions of PPMA in these systems ranged from 93% for the 10 wt % formulation to 99% for the 40 wt % system and yielded a series of four block copolymers whose PPPMA \bar{X}_n 's ranged from 49 to 57. The well-defined nature of the block copolymers is evidenced from their low dispersities and the unimodal, symmetric SEC traces (Figure 3). While the block copolymers have near identical composition, their macroscopic physical presentation varies considerably (Figure 3). In the case of the 10 and 20 wt % formulations, free-flowing solutions were obtained. In contrast, both the 30 and 40 wt % samples existed as physical gels at ambient temperature. As noted above, such differences in

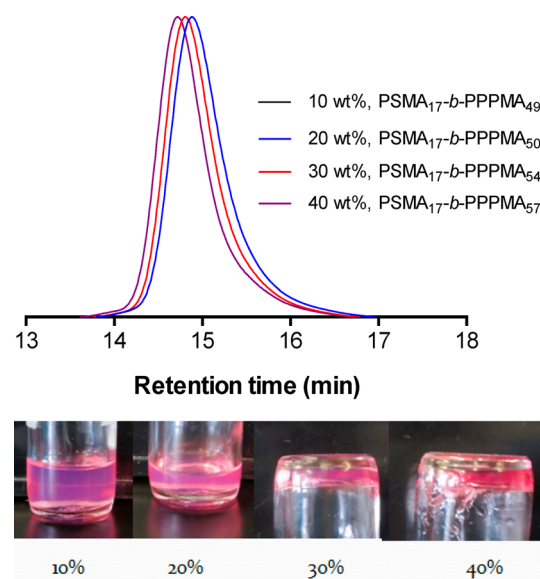


Figure 3. SEC traces of the PSMA₁₇-*b*-PPPMA_(49–57) copolymers demonstrating their unimodal nature (note the 10 and 20 wt % samples superimpose each other) and a series of digital pictures showing the change in macroscopic appearance with increasing total solids contents.

macroscopic appearance are generally associated with fundamental differences in the nanoparticle morphology with free-flowing solutions observed for spherical (or vesicular) species while gels are a common feature of nano-objects with a predominant worm morphology provided the sample is above some critical worm entanglement concentration. To evaluate the morphology, samples were extracted, diluted with *n*-tetradecane, stained with RuO₄, and imaged by TEM.

Figure 4 shows representative TEM images of these four samples at different total solids concentration. In the case of the

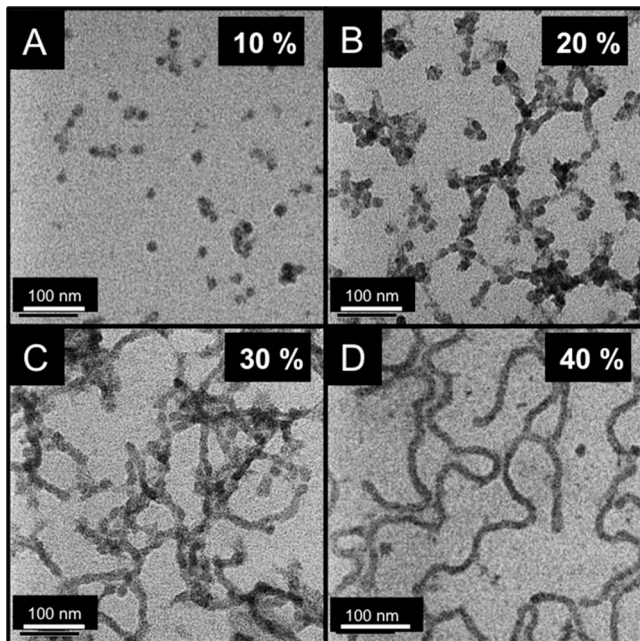


Figure 4. Representative TEM images of the PSMA₁₉-*b*-PPPMA_(49–57) copolymers prepared in *n*-tetradecane at variable total solids.

10 wt % sample, nanoparticles with a pure spherical shape were observed that had a DLS measured D_h of 22.8 nm, a value that is consistent with the TEM image shown. At 20 wt % we observe a phase that consists, primarily, of spheres although worms are clearly beginning to form but are not present at a concentration sufficient to result in macroscopic gelation. In contrast, at 30 wt % the morphology consists almost exclusively of worms (hence the gelation) while at 40 wt % we observe a pure worm phase with individual contour lengths of the worm aggregates on the order of multiple hundreds of nanometers.

Thermoreversible Polymorphism. We noted in Table 1 that the PSMA₁₉-*b*-PPPMA₈₅ sample prepared at 20 wt % solids formed a pure worm phase and existed as a soft physical gel at room temperature. The formation of a room temperature gel is due, fundamentally, to worm nanoparticle entanglements, a feature that has proven to be rather common in RAFTDP formulations in both polar and nonpolar media.^{17,30,36,40,46,47} Previously we have reported that such room temperature gels with PPPMA as the core-forming block can undergo degelation upon heating yielding a free-flowing solution and that this macroscopic change in appearance is accompanied by a fundamental change in the nanoparticle morphology from worms to spheres, the latter clearly being unable to form entanglements.^{30,35} Since the PSMA₁₉-*b*-PPPMA₈₅ copolymer existed as a gel at room temperature, we next examined if this species behaved in a similar manner. Previously, we noted that

for poly[2-(dimethylamino)ethyl methacrylate-*b*-PPMA] (PDMAEMA-*b*-PPPMA) copolymers prepared in ethanol (that formed pure worm phases) the macroscopic gel-to-solution physical transition occurred at ca. 70 °C over a very short time period of a few minutes. In contrast, heating the above gel to 70 °C and maintaining that temperature for 5 min did not result in any change in its macroscopic appearance except for a change in opacity; i.e., the sample was still a gel (Figure 5). Increasing the temperature to 85 °C (and holding

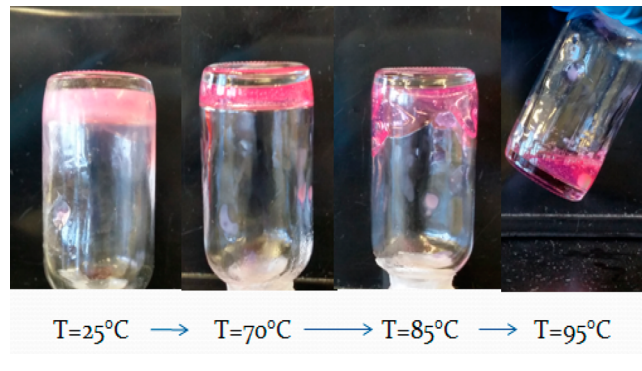


Figure 5. Change in physical appearance of the PSMA₁₉-*b*-PPPMA₈₅ copolymer sample with increasing temperature from 25 to 95 °C.

for 5 min) resulted in the partial disintegration of the gel, but it still did not form a total free-flowing solution. Finally, after heating at 95 °C for 5 min the sample presented as a free-flowing solution (Figure 5). As noted, we, and others, have shown previously that such changes in appearance are due, microscopically, to a change in the nanoparticle morphology. To check for similar behavior, aliquots were extracted from samples at 25 and 95 °C, diluted with *n*-tetradecane at the same temperature, stained, and imaged by TEM.

Figure 6 shows the TEM images of the polymeric nanoparticles obtained at these two different temperatures for

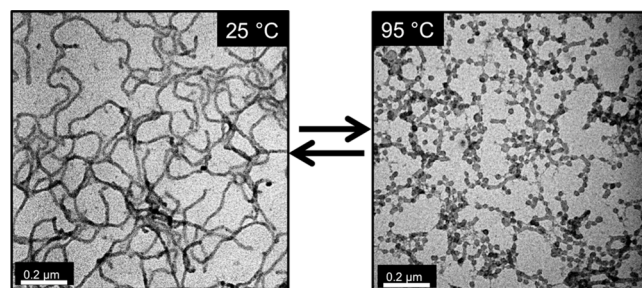


Figure 6. TEM images of the nanoparticles formed by the PSMA₁₉-*b*-PPPMA₈₅ copolymer at 25 and 95 °C demonstrating a thermally induced morphology change.

the PSMA₁₉-*b*-PPPMA₈₅ copolymer. As detailed above, at ambient temperature in *n*-tetradecane, this AB diblock copolymer existed in a pure worm phase with nanoparticle lengths of hundreds of nanometers being observed. In contrast, at 95 °C we observe nanoparticles with a predominant spherical morphology of reasonably narrow size distribution and an approximate size of ca. 30–50 nm. While there are some wormlike nano-objects still visible, they are more “oligomeric” in nature. We note that this thermal transition is completely reversible and cooling the 95 °C “solution” back to ambient temperature results in reformation of the gel state within a

matter of minutes. This morphological transition was also supported by DLS (Figure 7). At elevated temperature ($92\text{ }^{\circ}\text{C}$

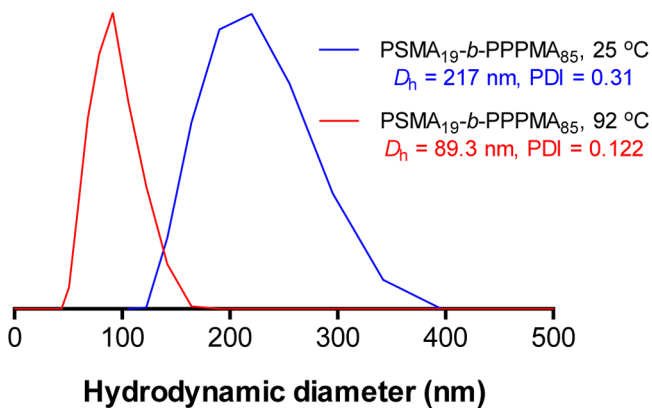


Figure 7. Intensity-average size distributions for the PSMA_{19} -*b*- PPPMA_{85} nanoparticles at 25 and $92\text{ }^{\circ}\text{C}$ as determined by dynamic light scattering.

in this instance) we observe a rather broad distribution whose intensity-average D_h is 89.3 nm and associated PDI of 0.122. In contrast, at room temperature temperature we see a dramatic increase in the intensity-average D_h to 217 nm (PDI = 0.31), an observation that is entirely consistent with the observed change in nanoparticle morphology highlighted above by TEM. We reiterate, however, given the assumptions associated with the Stokes–Einstein equation, this latter size should only be treated as a “sphere equivalent” value.

The exact physical cause for the (reversible) thermally induced morphology change is neither immediately obvious nor readily quantifiable. However, for such quick morphology changes to occur in these block copolymer systems the PPPMA core-forming block must be sufficiently mobile/solvated to facilitate rapid rearrangement. We noted above that the T_g for PPPMA has been determined to be $2\text{ }^{\circ}\text{C}$,³⁰ meaning that the core has amorphous characteristics at room temperature and above. This is a key physical feature (although technically a solid state property) since nanoparticles with core-forming blocks with high T_g 's, e.g., polystyrene, are generally considered kinetically frozen due to the highly crystalline or glassy natures of their cores.⁴⁸ However, it is important to note that a low T_g alone is not necessarily sufficient to facilitate rearrangement since other factors such as interfacial surface energy may still prohibit a morphology transition. Changes in the relative solvation of the core and coronal blocks that in turn may change the relative volume fractions of the blocks, and hence change p , can also be a contributing factor for effective rearrangement. We have previously demonstrated that in ethanolic PDMAEMA-*b*-PPPMA RAFTDP formulations that thermally reversible morphology changes are accompanied by changes in the solvation of the core PPPMA block at some critical temperature. Such changes in core, and or coronal, solvation are conveniently monitored by variable temperature ^1H NMR spectroscopy. The PSMA_{19} -*b*- PPPMA_{85} copolymer was analyzed by ^1H NMR spectroscopy in fully deuterated *n*-tetradecane, d_{30} -*n*-tetradecane, over the temperature range 25–105 °C (Figure 8). The key signals are those labeled a (the Ph hydrogens associated with the PPPMA side groups), d (the benzylic CH_2 group associated with the PPMA repeat units), and c (the CH_2 group directly adjacent to the ester groups in both the PSMA and PPPMA blocks). First, we note that we can

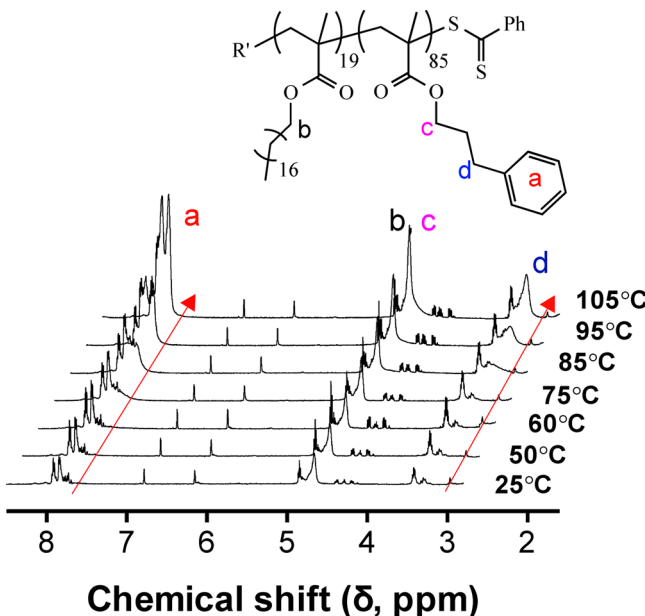


Figure 8. A series of ^1H NMR spectra recorded at increasing temperature in d_{30} -*n*-tetradecane for the PSMA_{19} -*b*- PPPMA_{85} copolymer highlighting the increasing solvation of the PPPMA block with increasing temperature. Measurements were made at a concentration of 0.5 wt %.

see these particular signals even at $25\text{ }^{\circ}\text{C}$, suggesting that the nanoparticle cores are not completely desolvated even under ambient conditions. However, the intensity of these signals in d_{30} -*n*-tetradecane do not change noticeably until the temperature reaches $85\text{ }^{\circ}\text{C}$ and then increase significantly at 95 and $105\text{ }^{\circ}\text{C}$. This is consistent, qualitatively, with the macroscopic observations (Figure 5), where physical degelation did not become visually obvious until the temperature reached $85\text{ }^{\circ}\text{C}$. This increasing solvation of the PPPMA block, and specifically the side groups, is clearly one of the driving forces for the observed facile macroscopic changes. Interestingly, the increasing solvation of the PPPMA block is not an “all-or-nothing” process. Figure 9 shows the relative integral values of those key resonances highlighted in Figure 8 assuming the intensity of the signals associated with the PSMA solvophilic block remain constant during the temperature ramping experiment. This clearly shows that the aromatic and benzylic functionalities become more solvated before those groups closer to the backbone, indicating a stepwise increase in the solvation of the core-forming PPPMA block. We also note that the block copolymer chains never become fully solvated, i.e., molecularly dissolved, since we observe spherical nanoparticles via TEM and clearly aggregated species by DLS at the elevated temperatures, indicating that the PPPMA block is still sufficiently solvophobic for self-assembly to occur. However, regardless of overall extent of PPPMA solvation, it is clearly intimately related to the thermally induced morphology transitions and is consistent with our previous work and that of Armes et al., who have performed similar NMR experiments when evaluating thermally induced morphology changes.^{30,36}

We also noted previously that while thermally induced degelation and its associated morphology transition is an interesting phenomenon, effective degelation can also be accomplished by simple dilution below the critical worm entanglement concentration (this does not necessarily imply a

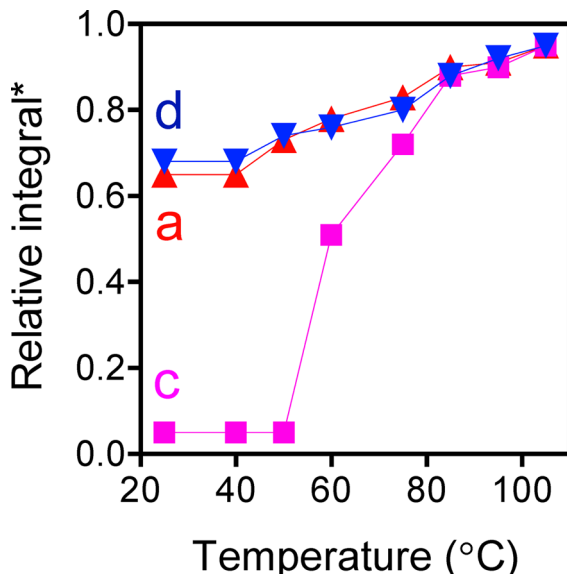


Figure 9. Relative integrals as a function of temperature for the $\text{PSMA}_{19}-b\text{-PPPMA}_{85}$ recorded in d_{30} -*n*-tetradecane for the key signals shown in Figure 8. The relative integral values are normalized using the absolute integral value of the vinyl proton peaks from residual monomer assuming the PSMA block is insensitive to increasing temperature.

change in morphology).³⁰ We note simply that such degelation can also be accomplished with the systems reported here by dilution with *n*-tetradecane. For example, a block copolymer forming a worm/gel phase at ambient temperature and 20 wt % solids could be transformed into a free-flowing solution by dilution to a critical value of 9 wt %.

CONCLUSIONS

Herein we have reported the first examples of RAFT dispersion polymerization (RAFTDP) in *n*-tetradecane with 3-phenylpropyl methacrylate (PPMA) as comonomer employing poly(stearyl methacrylate) (PSMA) as the solvophilic stabilizing species. $\text{PSMA}_x-b\text{-PPPMA}_y$ copolymer nanoparticles of varying morphology were readily prepared by under a range of different experimental conditions. At 20 wt % total solids with a PSMA_{19} macro-CTA, nanoparticles with spherical, worm, and vesicular morphologies are accessible simply by increasing the average degree of polymerization of the PPPMA block. Nanoparticle morphology can also be controlled by tuning the total solids content of the formulations for a fixed block copolymer composition although this is not as straightforward as the first approach. PSMA–PPPMA block copolymers of specific compositions existed as physical gels at room temperature—a macroscopic manifestation of microscopic worm nanoparticle entanglements. Degelation in such systems could be effected by heating to a critical temperature at which point samples became free-flowing solutions. This was shown to be due to a fundamental change in the nanoparticle morphology with the worm nano-objects converting to spheres. This temperature-induced morphology transition was completely reversible (cooling back to RT resulted in reformation of the gelled state). Effective transition between the two morphologies was demonstrated to be at least partly facilitated by an increase in the solvation of the core-forming PPPMA block.

AUTHOR INFORMATION

Corresponding Authors

*E-mail profandrewblowe@gmail.com (A.B.L.).

*E-mail yiwen.pei@unsw.edu.au (Y.P.).

Present Address

Y.P. and A.B.L.: Nanochemistry Research Institute (NRI) and Department of Chemistry, Curtin University, Bentley Campus, Bentley, Perth, WA 6102, Australia.

Notes

The authors declare no competing financial interest.

ACKNOWLEDGMENTS

A.B.L. thanks the Australian Research Council (ARC) for funding via the Future Fellowship program (FT110100046).

REFERENCES

- (1) Riess, G. *Prog. Polym. Sci.* **2003**, *28*, 1107–1170.
- (2) Antonietti, M.; Förster, S. *Adv. Mater.* **2003**, *15*, 1323–1333.
- (3) Cheng, J. Y.; Mayes, A. M.; Ross, C. A. *Nat. Mater.* **2004**, *3*, 823–828.
- (4) Discher, D. E.; Eisenberg, A. *Science* **2002**, *297*, 967–973.
- (5) Dreiss, C. A. *Soft Matter* **2007**, *3*, 956–970.
- (6) Du, J.; O'Reilly, R. K. *Soft Matter* **2009**, *5*, 3544–3561.
- (7) Gadt, T.; Jeong, N. S.; Cambridge, G.; Winnik, M. A.; Manners, I. *Nat. Mater.* **2009**, *8*, 144–150.
- (8) Holder, S. J.; Sommerdijk, N. A. J. M. *Polym. Chem.* **2011**, *2*, 1018–1028.
- (9) Howse, J. R.; Jones, R. A. L.; Battaglia, G.; Ducker, R. E.; Leggett, G. J.; Ryan, A. J. *Nat. Mater.* **2009**, *8*, 507–511.
- (10) Kita-Tokarczyk, K.; Grumelard, J.; Haefele, T.; Meier, W. *Polymer* **2005**, *46*, 3540–3563.
- (11) LaRue, I.; Adam, M.; Pitsikalis, M.; Hadjichristidis, N.; Rubinstein, M.; Sheiko, S. S. *Macromolecules* **2006**, *39*, 309–314.
- (12) Lim Soo, P.; Eisenberg, A. *J. Polym. Sci., Part B: Polym. Phys.* **2004**, *42*, 923–938.
- (13) Mai, Y.; Eisenberg, A. *Chem. Soc. Rev.* **2012**, *41*, 5969–5985.
- (14) Rodriguez Hernandez, J.; Checot, F.; Gnanou, Y.; Lecommandoux, S. *Prog. Polym. Sci.* **2005**, *30*, 691–724.
- (15) Sun, J.-T.; Hong, C.-Y.; Pan, C.-Y. *Polym. Chem.* **2013**, *4*, 873–881.
- (16) Wan, W.-M.; Pan, C.-Y. *Polym. Chem.* **2010**, *1*, 1475–1484.
- (17) Warren, M. J.; Armes, S. P. *J. Am. Chem. Soc.* **2014**, *136*, 10174–10185.
- (18) Charleux, B.; Delaittre, G.; Rieger, J.; D'Agosto, F. *Macromolecules* **2012**, *45*, 6753–6765.
- (19) Wan, W. M.; Sun, X. L.; Pan, C. Y. *Macromol. Rapid Commun.* **2010**, *31*, 399–404.
- (20) Huang, C.-Q.; Pan, C.-Y. *Polymer* **2010**, *51*, 5115–5121.
- (21) He, W.-D.; Sun, X.-L.; Wan, W.-M.; Pan, C.-Y. *Macromolecules* **2011**, *44*, 3358–3365.
- (22) Rieger, J.; Grazon, C.; Charleux, B.; Alaimo, D.; Jérôme, C. J. *J. Polym. Sci., Part A: Polym. Chem.* **2009**, *47*, 2373–2390.
- (23) Sugihara, S.; Blanazs, A.; Armes, S. P.; Ryan, A. J.; Lewis, A. L. *J. Am. Chem. Soc.* **2011**, *133*, 15707–15713.
- (24) Semsarilar, M.; Ladmiral, V.; Blanazs, A.; Armes, S. P. *Langmuir* **2013**, *29*, 7416–7424.
- (25) Semsarilar, M.; Jones, E. R.; Blanazs, A.; Armes, S. P. *Adv. Mater.* **2012**, *24*, 3378–3382.
- (26) Li, Y.; Armes, S. P. *Angew. Chem., Int. Ed.* **2010**, *49*, 4042–4046.
- (27) Ladmiral, V.; Semsarilar, M.; Canton, I.; Armes, S. P. *J. Am. Chem. Soc.* **2013**, *135*, 13574–13581.
- (28) Blanazs, A.; Ryan, A. J.; Armes, S. P. *Macromolecules* **2012**, *45*, 5099–5107.
- (29) Pei, Y.; Lowe, A. B. *Polym. Chem.* **2014**, *5*, 2342–2351.
- (30) Pei, Y.; Dharsana, N. C.; van Hensbergen, J. A.; Burford, R. P.; Roth, P. J.; Lowe, A. B. *Soft Matter* **2014**, *10*, 5787–5796.

- (31) Pei, Y.; Dharsana, N. C.; Lowe, A. B. *Aust. J. Chem.* **2015**, DOI: 10.1072/CH14490.
- (32) He, X.; Li, Q.; Shi, P.; Cui, Y.; Li, S.; Zhang, W. *Polym. Chem.* **2014**, *5*, 7090–7099.
- (33) Houillot, L.; Bui, C.; Farcet, C.; Moire, C.; Raust, J. A.; Pasch, H.; Save, M.; Charleux, B. *ACS Appl. Mater. Interfaces* **2010**, *2*, 434–442.
- (34) Fielding, L. A.; Derry, M. J.; Ladmiral, V.; Rosselgong, J.; Rodrigues, A. M.; Ratcliffe, L. P. D.; Sugihara, S.; Armes, S. P. *Chem. Sci.* **2013**, *4*, 2081–2087.
- (35) Pei, Y.; Sugita, O.; Thurairajah, L.; Lowe, A. B. *Polym. Chem.*, submitted.
- (36) Fielding, L. A.; Lane, J. A.; Derry, M. J.; Mykhaylyk, O. O.; Armes, S. P. *J. Am. Chem. Soc.* **2014**, *136*, 5790–5798.
- (37) Zong, M.; Thurecht, K. J.; Howdle, S. M. *Chem. Commun.* **2008**, 5942–5944.
- (38) Jennings, J.; Beija, M.; Kennon, J. T.; Willcock, H.; O'Reilly, R. K.; Rimmer, S.; Howdle, S. M. *Macromolecules* **2013**, *46*, 6843–6851.
- (39) Dan, M.; Huo, F.; Xiao, X.; Su, Y.; Zhang, W. *Macromolecules* **2014**, *47*, 1360–1370.
- (40) Lovett, J. R.; Warren, N. J.; Ratcliffe, L. P.; Kocik, M. K.; Armes, S. P. *Angew. Chem., Int. Ed.* **2014**, DOI: 10.1002/anie.201409799.
- (41) Chambon, P.; Blanazs, A.; Battaglia, G.; Armes, S. P. *Macromolecules* **2012**, *45*, 5081–5090.
- (42) Ratcliffe, L. P. D.; Blanazs, A.; Williams, C. N.; Brown, S. L.; Armes, S. P. *Polym. Chem.* **2014**, *5*, 3643–3655.
- (43) Israelachvili, J. N.; Mitchell, D. J.; Ninham, B. W. *J. Chem. Soc., Faraday Trans. 2* **1976**, *72*, 1525–1568.
- (44) Abbas, S.; Li, Z.; Hassan, H.; Lodge, T. P. *Macromolecules* **2007**, *40*, 4048–4052.
- (45) Blanazs, A.; Madsen, J.; Battaglia, G.; Ryan, A. J.; Armes, S. P. *J. Am. Chem. Soc.* **2011**, *133*, 16581–16587.
- (46) Raghavan, S. R.; Douglas, J. F. *Soft Matter* **2012**, *8*, 8539–8546.
- (47) Verber, R.; Blanazs, A.; Armes, S. P. *Soft Matter* **2012**, *8*, 9915–9922.
- (48) Nicolai, T.; Colombani, O.; Chassenieux, C. *Soft Matter* **2010**, *6*, 3111–3118.